Adaptive Per-Distance Sampling for Efficient Multi-Scale Network Centrality Analysis

Author Name
Affiliation
email@example.com

January 23, 2026

Abstract

Computing network centrality measures across multiple distance thresholds is fundamental to urban morphology analysis but computationally expensive for large networks. We present an adaptive sampling approach that automatically calibrates sampling probability for each distance threshold based on network reachability. Our key insight is that *effective sample size*—the product of mean reachability and sampling probability—determines both ranking accuracy (Spearman ρ) and magnitude accuracy across network topologies. Through experiments on synthetic networks representing urban cores, suburban areas, and transit corridors, we fit empirical models predicting accuracy from effective sample size for both shortest path (metric) and simplest path (angular) distance heuristics. We find that betweenness centrality requires approximately 1.5× more samples than harmonic closeness for equivalent accuracy with shortest paths, while angular distances exhibit distinct behaviour: angular harmonic converges faster (requiring half the samples) but angular betweenness has higher variance (requiring 27% more samples). Our adaptive algorithm achieves approximately 2× speedup while maintaining $\rho \geq 0.95$ across all distance thresholds, compared to uniform sampling which fails to maintain accuracy at short distances. We validate our approach on real-world street networks from London and Madrid, demonstrating that the empirical models generalise beyond synthetic test cases. The implementation is available as part of the open-source `cityseer` Python library.

Keywords: network centrality, sampling, urban morphology, betweenness, closeness, computational efficiency

1 Introduction

Network centrality measures are fundamental tools for understanding urban morphology, identifying key locations in street networks, and informing urban planning decisions (Porta et al., 2006; Boeing, 2017). Measures such as betweenness centrality (which captures through-movement potential) and closeness centrality (which captures accessibility) have been widely applied to characterise pedestrian-scale urban environments (Hillier and Hanson, 1984; Cooper, 2015).

A key methodological advance in urban network analysis is the use of *localised* or *distance-bounded* centrality measures, where centrality is computed within a specified network distance rather than across the entire graph (Cooper, 2015). While early applications focused on pedestrian-scale analysis within walking distance (500m–2000m), contemporary urban analytics increasingly requires *regional-scale* analysis at distances of 5–20km. Such analyses are essential for:

- **Cycling infrastructure planning**: Identifying strategic routes and connectivity gaps at distances of 5–15km

- **Transit accessibility**: Evaluating station catchments and transfer patterns across metropolitan regions
- **Regional economic analysis**: Understanding accessibility to employment centres and services
- **Multi-modal integration**: Combining pedestrian, cycling, and transit networks in unified analyses

Multi-scale analysis—computing centrality at multiple distance thresholds spanning local to regional scales—enables researchers to capture accessibility patterns across spatial scales relevant to different transport modes and planning questions.

1.1 The Computational Challenge

Multi-scale centrality computation is computationally expensive. For a network with n nodes and d distance thresholds, naïve computation requires $O(n^2 \cdot d)$ shortest-path calculations. To illustrate the practical implications:

- A **neighbourhood-scale network** (5,000 nodes, 4 distances) requires ∼100 million path calculations
- A **city-scale network** (50,000 nodes, 4 distances) requires ∼10 billion path calculations
- A **metropolitan-scale network** (200,000 nodes, 6 distances) requires ∼240 billion path calculations

Even with optimised implementations, city-scale analyses can require hours of computation, while metropolitan-scale analyses may be impractical without approximation methods. This computational burden limits the ability of researchers and practitioners to iterate rapidly, explore parameter sensitivity, or integrate network analysis into interactive planning tools.

1.2 Sampling-Based Approximation

A natural approach to reducing computational cost is *sampling*: rather than computing shortest paths from all nodes, we sample a subset of source nodes and extrapolate. This approach has been explored extensively for betweenness centrality (Brandes and Pich, 2007; Riondato and Kornaropoulos, 2016), but less attention has been paid to multi-scale, distance-bounded centrality computation.

The key insight is that sampling becomes increasingly effective at longer distances. At a 20km threshold in a metropolitan network, each node may be reachable from 50,000+ other nodes. Computing exact centrality requires shortest-path calculations from all 50,000 sources, but sampling just 2% of sources (1,000 nodes) can yield highly accurate estimates—because the statistical power comes from the large number of source-target pairs, not the proportion sampled.

However, the challenge with sampling in the multi-scale context is that a *uniform* sampling probability fails to provide consistent accuracy across distance thresholds. At short distances (e.g., 500m), typical urban networks have low *reachability*—perhaps only 100–300 nodes. Sampling 2% would yield just 2–6 source nodes per estimate, resulting in unacceptably high variance. At long distances, the same 2% provides excellent accuracy but may still be more computation than necessary.

1.3 Contributions

This paper presents an *adaptive per-distance sampling* approach that addresses this tension. Our contributions are:

1. We introduce the concept of *effective sample size*, n_{eff} = reachability $\times$ p, and demonstrate empirically that this quantity determines both ranking accuracy (Spearman ρ) and magnitude accuracy across diverse network topologies.
2. We fit empirical models predicting accuracy from effective sample size for both harmonic closeness and betweenness centrality. Notably, we find that betweenness requires approximately 1.5$\times$ more samples than closeness for equivalent accuracy due to higher variance.
3. We present an adaptive algorithm that probes network reachability at each distance threshold and calibrates sampling probability to achieve a target accuracy level (e.g., $\rho \geq 0.95$).
4. We validate our approach on both synthetic networks representing archetypal urban forms (grid, dendritic, linear) and real-world street networks from London and Madrid.
5. We provide an open-source implementation integrated into the `cityseer` Python library for urban network analysis.

The remainder of this paper is organised as follows. Section 2 reviews related work on network centrality and sampling methods. Section 3 describes our experimental methodology. Section 4 presents the fitted empirical models. Section 5 describes the adaptive sampling algorithm. Section 6 presents validation results on synthetic and real-world networks. Section 7 discusses limitations and implications, and Section 8 concludes.

2 Background and Related Work

2.1 Foundations of Network Centrality

Network centrality measures quantify the relative importance of nodes within a graph structure. The concept originated in social network analysis, with Bavelas (1950) first proposing that communication efficiency in groups depends on the structural position of individuals. Sabidussi (1966) formalised closeness centrality as the reciprocal of the sum of distances to all other nodes, while Freeman (1977) introduced betweenness centrality based on the fraction of shortest paths passing through a node. Freeman's subsequent conceptual clarification (Freeman, 1979) established the theoretical framework that remains foundational to centrality analysis across disciplines.

Betweenness centrality measures how often a node lies on shortest paths between other nodes:

$$C_B(v) = \sum_{s \neq v \neq t} \frac{\sigma_{st}(v)}{\sigma_{st}} \tag{1}$$

where σ_{st} is the number of shortest paths from s to t, and $\sigma_{st}(v)$ is the number passing through v. High betweenness indicates locations with high through-movement potential—nodes that serve as bridges or bottlenecks in the network.

Closeness centrality measures proximity to all other nodes. The classic formulation by Sabidussi (1966) uses the reciprocal of total distance, but this is undefined for disconnected graphs. Following Marchiori and Latora (2000), who showed that the harmonic mean behaves better than the arithmetic mean for networks with infinite distances, the *harmonic closeness* variant has gained widespread adoption (Rochat, 2009; Boldi and Vigna, 2014):

$$C_H(v) = \sum_{u \neq v} \frac{1}{d(v,u)} \tag{2}$$

where $d(v, u)$ is the shortest-path distance from v to u. Boldi and Vigna (2014) provided axiomatic foundations showing that harmonic centrality uniquely satisfies desirable properties for centrality measures, including proper handling of unreachable nodes.

2.2 Centrality in Urban Street Networks

The application of network centrality to urban analysis emerged from two parallel traditions. In the *space syntax* tradition, Hillier and Hanson (1984) developed configurational analysis methods based on the insight that spatial layout influences pedestrian movement patterns. Their "natural movement" theory (Hillier et al., 1993) demonstrated strong correlations between network integration (a topological centrality measure) and observed pedestrian flows.

The *complex networks* tradition, drawing on physics and network science (Watts and Strogatz, 1998; Barabási and Albert, 1999), brought metric-based centrality analysis to urban streets. Porta et al. (2006) introduced "multiple centrality assessment" (MCA), applying degree, closeness, betweenness, and other centrality measures to primal graph representations of urban streets using metric rather than topological distance. Crucitti et al. (2006) analysed 18 cities worldwide, finding that self-organised cities exhibit scale-free centrality distributions while planned cities do not.

Modern urban network analysis tools—including OSMnx (Boeing, 2017, 2021), Urban Network Analysis (Sevtsuk and Mekonnen, 2012), sDNA (Cooper and Chiaradia, 2018), and `cityseer` (Simons, 2022)—enable large-scale computation of centrality metrics on street networks derived from OpenStreetMap and other sources.

2.3 Localised Centrality Measures

Traditional centrality measures consider the entire network, but pedestrian behaviour is influenced primarily by local accessibility within walking distance. Cooper (2015) formalised *localised* or *distance-bounded* centrality measures that restrict computation to nodes within a distance threshold r:

$$C_H^r(v) = \sum_{\substack{u \neq v \\ d(v,u) \leq r}} \frac{1}{d(v, u)} \tag{3}$$

This localisation addresses what Cooper termed a "self-contradictory but useful" aspect of centrality—that global measures may not reflect local accessibility patterns relevant for pedestrian-scale analysis. Multi-scale analysis, computing centrality at multiple distance thresholds (e.g., 500m, 1000m, 2000m, 5000m), has become standard practice for capturing both immediate neighbourhood accessibility and broader urban connectivity (Turner, 2007).

2.4 Computational Complexity and the Brandes Algorithm

The computational cost of centrality measures limited early applications. Computing betweenness exactly required $O(n^3)$ time until Brandes (2001) introduced an algorithm running in $O(nm)$ time for unweighted graphs and $O(nm+n^2 \log n)$ for weighted graphs. This breakthrough, which accumulates betweenness scores during single-source shortest-path computations, remains the foundation for exact betweenness computation (Brandes, 2008).

However, for multi-scale localised centrality with d distance thresholds, the naive approach requires $O(n^2 d)$ shortest-path computations. For large urban networks with tens or hundreds of thousands of nodes, this remains prohibitive, especially when rapid iteration is needed for planning applications.

2.5 Sampling-Based Approximation

Sampling-based approximation offers a path to tractable computation. The key insight is that centrality can be estimated by computing shortest paths from a *sample* of source nodes rather than all nodes.

Pivot-based sampling. Brandes and Pich (2007) showed that sampling k uniformly random "pivots" and scaling by n/k produces an unbiased estimator. They tested various sampling strategies (random, degree-proportional, maximising distance from previous pivots) and found that uniformly random sampling performs best. The expected error decreases proportionally to $1/\sqrt{k}$.

Adaptive sampling. Bader et al. (2007) introduced adaptive sampling that adjusts the number of samples based on information obtained during computation. Their method achieves smaller sample sizes for high-centrality nodes, where fewer samples suffice for accurate estimation.

VC-dimension bounds. Riondato and Kornaropoulos (2014, 2016) provided the first theoretically-grounded sample size bounds using Vapnik-Chervonenkis (VC) dimension theory from statistical learning. By proving that the VC-dimension of the associated range space depends only on the *vertex diameter* (maximum number of nodes in any shortest path), not on graph size, they obtained sample sizes guaranteeing (ϵ, δ)-approximation—that is, all estimates within additive error ϵ with probability at least $1 - \delta$.

Advanced algorithms. Borassi and Natale (2016, 2019) developed KADABRA (ADaptive Algorithm for Betweenness via Random Approximation), which combines efficient shortest-path sampling with adaptive stopping criteria. Comparative benchmarks (Bergamini et al., 2019) found KADABRA to be among the best-performing algorithms across diverse network types.

Closeness approximation. Less attention has been paid to closeness centrality approximation. Cohen et al. (2014) proposed a hybrid sampling-pivoting algorithm for classic closeness that achieves near-linear time complexity with bounded relative error.

2.6 Gap in Existing Literature

Prior work on sampling for centrality has focused predominantly on:

- **Global centrality**: Measures computed over the entire network, not localised to distance thresholds
- **Single-scale computation**: Fixed analysis scope rather than multi-scale approaches
- **Betweenness centrality**: With comparatively less attention to harmonic closeness
- **Theoretical bounds**: Sample sizes derived from worst-case analysis, which may be conservative for practical networks
- **Network-independent guarantees**: Bounds that do not account for network topology characteristics

The specific challenge of *multi-scale localised centrality*—where different distance thresholds have fundamentally different reachability characteristics—has received little attention. At short distances, typical urban networks have low reachability (few nodes within threshold), while at long distances, reachability can approach the full network size. Uniform sampling fails in this setting because a fixed sampling probability that works well at long distances provides insufficient samples at short distances.

Our work addresses this gap by:

1. Introducing *effective sample size* as a unifying concept that explains accuracy across diverse topologies and distance thresholds

2. Fitting separate empirical models for harmonic closeness and betweenness, revealing that betweenness requires approximately 1.5× more samples for equivalent accuracy

3. Developing an *adaptive per-distance* algorithm that calibrates sampling probability independently for each distance threshold

4. Validating on both synthetic networks and real-world street networks from London and Madrid

3 Methodology

3.1 Experimental Design

We conduct experiments on both synthetic and real-world networks to understand the relationship between sampling parameters and accuracy.

3.1.1 Synthetic Networks

We generate three synthetic network topologies representing archetypal urban forms (Figure 1):

- **Trellis**: Dense grid-like networks characteristic of urban cores with high connectivity
- **Tree**: Branching dendritic networks characteristic of suburban areas with hierarchical structure
- **Linear**: Corridor networks characteristic of transit routes with low transverse connectivity

Each network is generated as a 3×3 tile pattern with approximately 2940m network extent.

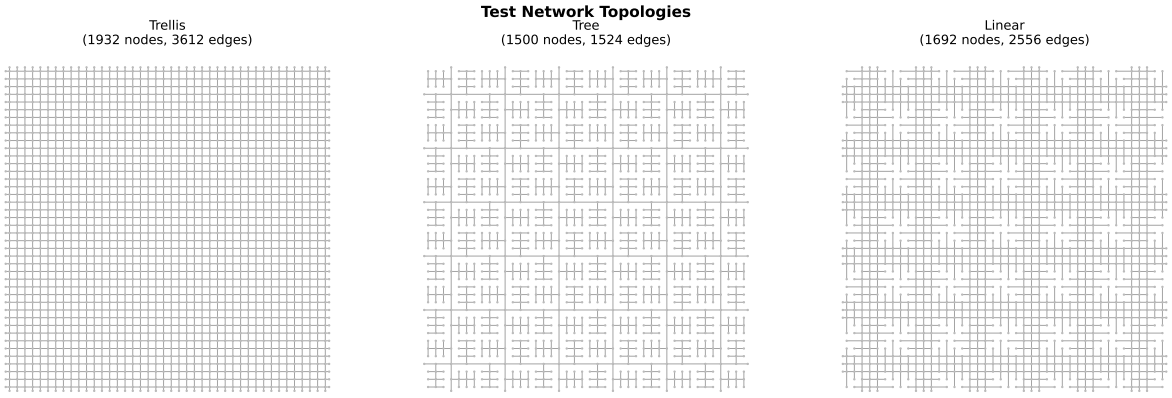

Figure 1: Synthetic network topologies representing archetypal urban forms: trellis (dense grid), tree (dendritic/suburban), and linear (corridor). Each topology is generated as a 3×3 tile pattern.

3.1.2 Real-World Networks

We validate on street networks downloaded from OpenStreetMap representing diverse urban forms:

- **London (Soho)**: Dense, irregular historical street pattern
- **Madrid (Centro)**: Mediterranean grid with radial elements

- **Phoenix (Scottsdale)**: American suburban sprawl with cul-de-sacs and low connectivity

Networks are extracted using the `cityseer` library with automatic simplification and cleaning. The network structures are visible in Figure 8, which shows the spatial distribution of nodes for each city.

3.2 Centrality Computation

We compute two localised centrality measures:

1. **Harmonic closeness**: Sum of inverse distances to nodes within threshold
2. **Betweenness**: Count of shortest paths through each node, restricted to source-target pairs within threshold

3.2.1 Distance Heuristics

Both metrics can be computed using different distance heuristics:

- **Shortest path (metric)**: Traditional distance-minimising paths using physical edge lengths. This captures accessibility based on travel distance.
- **Simplest path (angular)**: Paths that minimise cumulative angular change at intersections. Following Turner (2007), we compute angular change at each turn and accumulate a cost proportional to the deviation from straight-ahead travel. This captures movement patterns that favour "legible" routes requiring fewer direction changes.

The angular heuristic aligns with space syntax's emphasis on cognitive aspects of navigation, while shortest paths align with traditional transport accessibility. We fit separate empirical models for each heuristic, as they exhibit different variance characteristics.

Implementation uses Dijkstra's algorithm with distance-bounded search, implemented in Rust for performance.

3.3 Accuracy Metrics

We evaluate accuracy along two dimensions:

3.3.1 Ranking Accuracy (Spearman ρ)

The primary accuracy metric is Spearman's rank correlation coefficient between true (full computation) and estimated (sampled) centrality values:

$$\rho_{\text{sp}} = 1 - \frac{6 \sum_i (r_i - \hat{r}_i)^2}{n(n^2 - 1)} \tag{4}$$

where r_i and $\hat{r}_i$ are the ranks of node i under true and estimated centrality. A value of $\rho_{\text{sp}} = 1$ indicates perfect ranking preservation.

Ranking accuracy is the most important metric for typical urban analysis applications, where researchers identify "high centrality" or "low centrality" locations rather than interpreting absolute values.

3.3.2 Magnitude Accuracy (Scale Ratio)

We also measure the scale ratio between estimated and true values:

$$\text{scale} = \text{median}\left(\frac{\hat{C}(v)}{C(v)}\right) \tag{5}$$

A scale ratio of 1.0 indicates no systematic bias. Values below 1.0 indicate underestimation.

3.4 Effective Sample Size

The key insight motivating our approach is that accuracy depends on *effective sample size*:

$$n_{\text{eff}} = \bar{R} \times p \tag{6}$$

where $\bar{R}$ is the mean reachability (average number of nodes reachable within the distance threshold) and p is the sampling probability.

Equation 6 captures the intuition that each node's centrality estimate is derived from contributions by approximately n_{eff} sampled source nodes. When n_{eff} is small, estimates have high variance; when n_{eff} is large, estimates are reliable.

Table 1 provides a lookup showing n_{eff} for various combinations of reachability and sampling probability. The highlighted cells indicate configurations achieving $n_{\text{eff}} \geq 400$, which corresponds to $\rho_{\text{sp}} \approx 0.90$ for betweenness centrality (shortest path).

Table 1: Effective sample size ($n_{\text{eff}} = \bar{R} \times p$) for various reachability and sampling probability combinations. Bold values indicate $n_{\text{eff}} \geq 400$, yielding $\rho_{\text{sp}} \geq 0.90$.

Reachability	$p = 10\%$	$p = 20\%$	$p = 30\%$	$p = 40\%$	$p = 50\%$
100	10	20	30	40	50
200	20	40	60	80	100
400	40	80	120	160	200
800	80	160	240	320	**400**
1000	100	200	300	**400**	**500**
2000	200	**400**	**600**	**800**	**1000**

3.5 Experimental Parameters

Table 2: Experimental parameters for sampling accuracy analysis.

Parameter	Value
Topologies	Trellis, Tree, Linear
Tiles	5
Distances	500, 1000, 2000, 5000m
Sampling probabilities	0.05, 0.10, 0.15, 0.20, 0.30, 0.50, 0.70, 1.00
Runs per configuration	10

For each configuration (topology × distance × probability), we run 20 independent trials with different random seeds to estimate variance.

3.6 Correctness Verification

Before analysing sampling effects, we verify that `cityseer`'s centrality implementation matches NetworkX (the reference implementation). All metrics pass verification with maximum differences below 10^{-6}:

Table 3: Verification that full computation ($p = 1.0$) produces identical results.

Metric	Full ρ	Expected
Harmonic Closeness	1.000	1.000
Betweenness	1.000	1.000

4 Empirical Models

4.1 Model Form

Based on the experimental data, we fit empirical models predicting accuracy from effective sample size. We use a hyperbolic model form:

$$\rho_{\text{sp}} = 1 - \frac{A}{B + n_{\text{eff}}} \tag{7}$$

This form has desirable properties:

- Approaches 1.0 as $n_{\text{eff}} \to \infty$ (perfect accuracy with infinite samples)
- Bounded below (accuracy cannot be negative)
- Captures diminishing returns at high n_{eff}

4.2 Fitting Procedure

We fit separate models for harmonic closeness and betweenness centrality, as initial analysis revealed different variance characteristics between the metrics. We also fit separate models for shortest path (metric) distances and simplest path (angular) distances, as these distance heuristics exhibit different accuracy characteristics.

To provide *conservative* estimates suitable for practical use, we fit to the 10th percentile of observed accuracy within effective sample size bins, rather than the mean. This ensures that the model predictions represent a lower bound on expected accuracy, accounting for topology-dependent variation.

4.3 Fitted Model Parameters

Table 4: Fitted model parameters for predicting Spearman ρ from effective sample size ($\rho = 1 - A/(B + n_{\text{eff}})$). Models fitted to 10th percentile for conservative estimates. Shortest path models apply to metric distance functions; angular models apply to simplest path (angular) distance functions.

Distance	Metric	A	B	RMSE	n_{eff} for $\rho = 0.95$	n_{eff} for $\rho = 0.99$
Shortest	Harmonic	32.30	31.45	0.041	615	3199
Shortest	Betweenness	48.31	49.12	0.049	917	4782
Angular	Harmonic	16.87	16.13	0.030	321	1671
Angular	Betweenness	61.46	61.36	0.046	1168	6085

The results reveal several key differences between metrics and distance heuristics:

4.3.1 Metric Differences

The betweenness model has larger coefficients than harmonic closeness, reflecting higher variance and the need for more samples to achieve equivalent accuracy. This is consistent across both distance types.

4.3.2 Distance Heuristic Differences

Angular (simplest path) distances show markedly different behaviour from shortest path distances:

- **Angular harmonic closeness** converges faster than shortest-path harmonic, requiring only $n_{\text{eff}} \geq 321$ for $\rho_{\text{sp}} = 0.95$ compared to $n_{\text{eff}} \geq 615$ for shortest paths—approximately half the samples
- **Angular betweenness** exhibits higher variance than shortest-path betweenness, requiring $n_{\text{eff}} \geq 1168$ for $\rho_{\text{sp}} = 0.95$ compared to $n_{\text{eff}} \geq 917$—approximately 27% more samples

This difference reflects the nature of angular distance computation: angular paths preferentially follow straight routes, concentrating betweenness on fewer "through-movement" corridors. This increases variance in betweenness estimates (high values are more sensitive to sampling), while angular closeness benefits from the smoother accumulation of inverse distances along fewer candidate paths.

4.4 Additional Models

We also fit models for uncertainty (standard deviation) and magnitude bias:

4.4.1 Standard Deviation Model

$$\sigma = \frac{C}{\sqrt{D + n_{\text{eff}}}} \tag{8}$$

This captures the expected $1/\sqrt{n}$ convergence rate from sampling theory.

4.4.2 Magnitude Bias Model

$$\text{scale} = 1 - \frac{E}{F + n_{\text{eff}}} \tag{9}$$

This captures the observed tendency for sampling to underestimate magnitudes at low n_{eff}.

4.5 Model Validation

Figures 2 and 3 show observed accuracy versus effective sample size for shortest and angular distances, respectively. The models capture the central tendency well across all configurations.

4.6 Inverting the Model

For practical use, we need to compute the required effective sample size for a target accuracy level. Inverting Equation 7:

$$n^*_{\text{eff}} = \frac{A}{1 - \rho^*_{\text{sp}}} - B \tag{10}$$

Given target ρ^*_{sp} and observed reachability $\bar{R}$, the required sampling probability is:

$$p^* = \frac{n^*_{\text{eff}}}{\bar{R}} = \frac{1}{\bar{R}} \left(\frac{A}{1 - \rho^*_{\text{sp}}} - B \right) \tag{11}$$

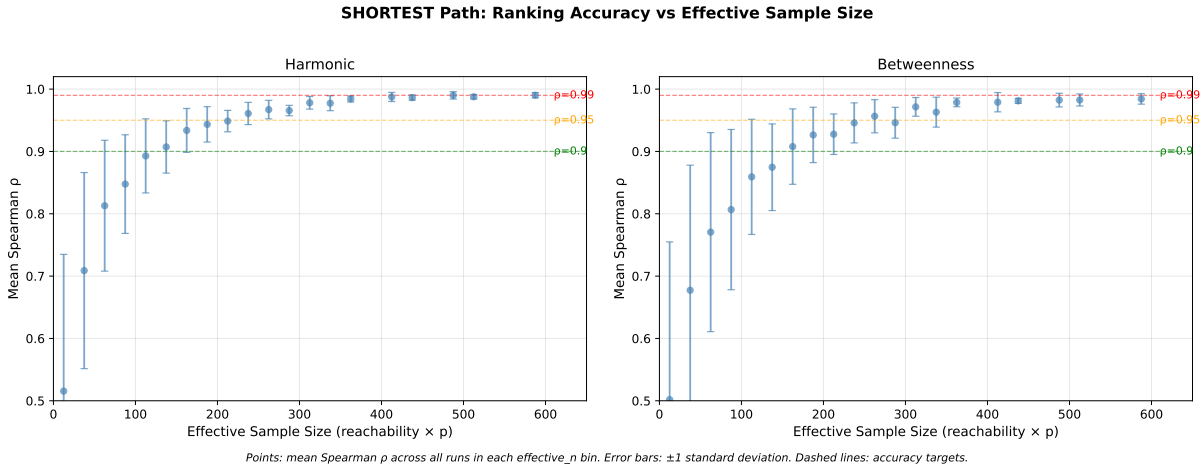

Figure 2: Observed Spearman ρ versus effective sample size for **shortest path** (metric) distances. Left: harmonic closeness. Right: betweenness. Points are coloured by network topology. Solid lines show fitted models (10th percentile). Dashed horizontal lines indicate common accuracy targets.

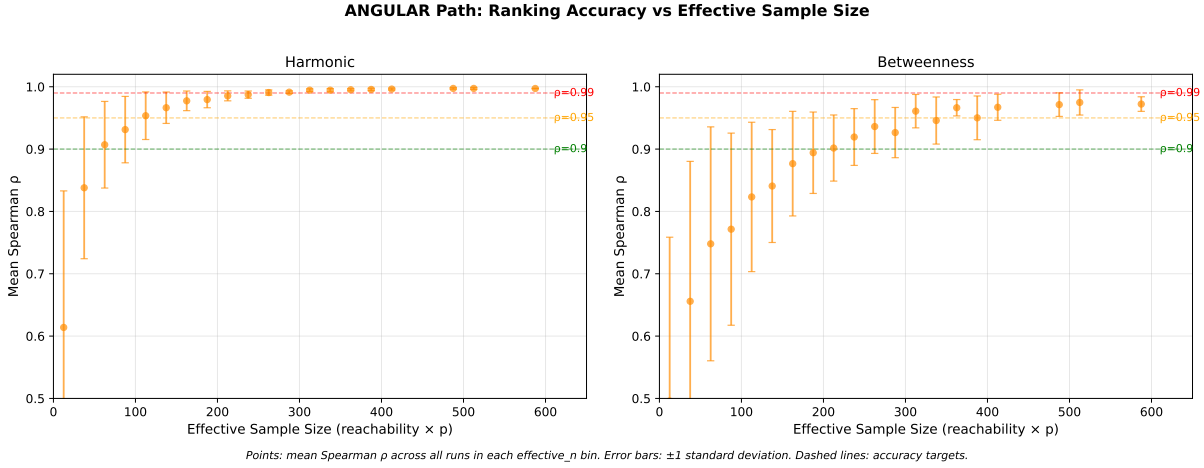

Figure 3: Observed Spearman ρ versus effective sample size for **angular** (simplest path) distances. Left: harmonic closeness. Right: betweenness. Note the faster convergence for harmonic closeness and higher variance for betweenness compared to shortest path distances (Figure 2).

Figures 4 and 5 show the required sampling probability for various target accuracy levels as a function of network reachability, for shortest and angular distances respectively.

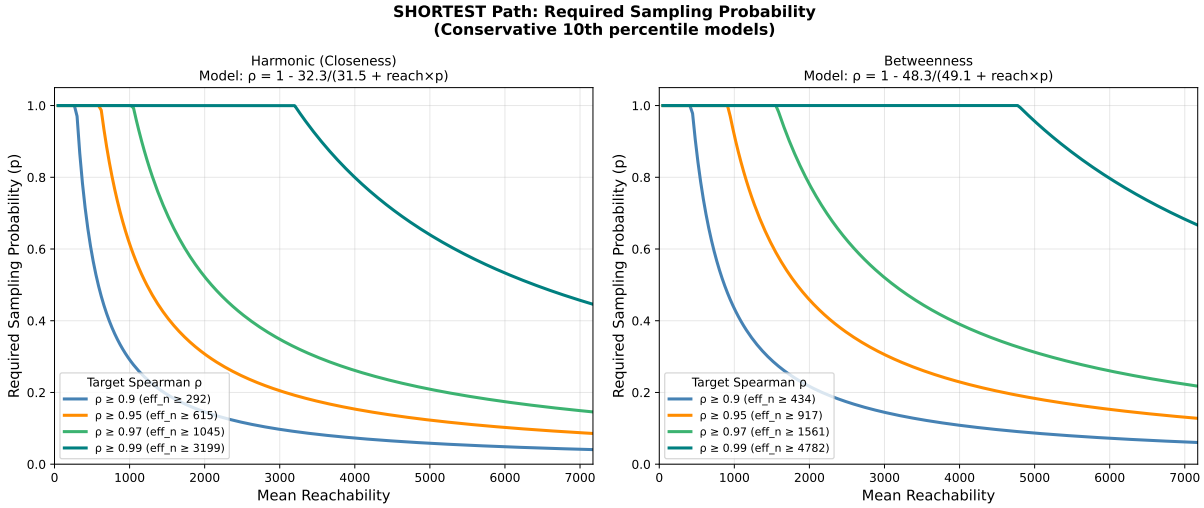

Figure 4: Required sampling probability for **shortest path** distances to achieve target accuracy levels ($\rho = 0.90, 0.95, 0.97, 0.99$) as a function of mean network reachability. Based on the betweenness (conservative) model.

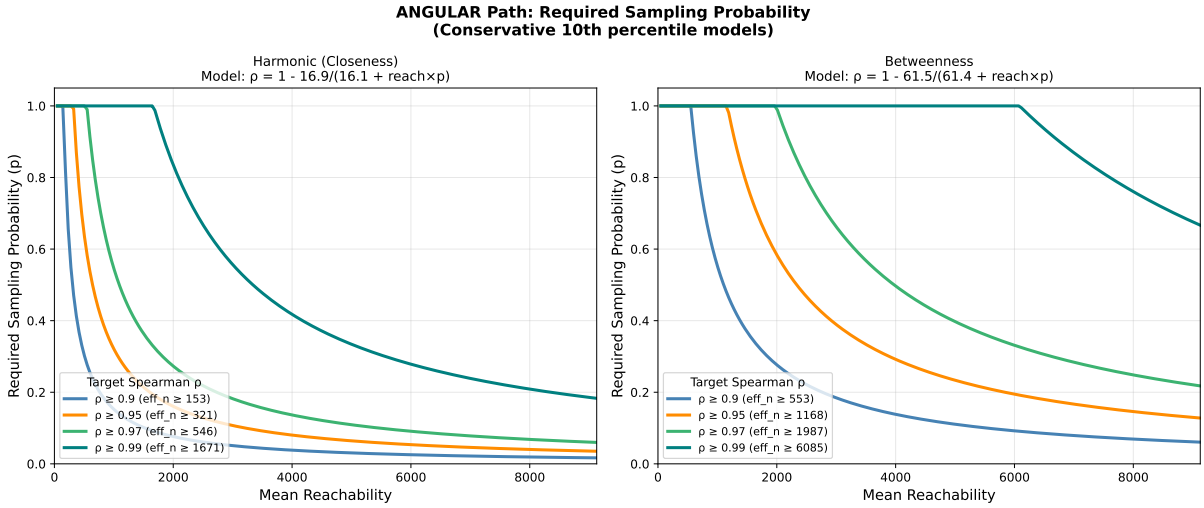

Figure 5: Required sampling probability for **angular** (simplest path) distances to achieve target accuracy levels. The angular betweenness model requires higher sampling probabilities than shortest-path betweenness due to the increased variance from angular path concentration.

5 Adaptive Sampling Algorithm

5.1 Problem Statement

Given a network $G = (V, E)$, a set of distance thresholds $\{r_1, r_2, \ldots, r_d\}$, and a target accuracy ρ^*_{sp}, compute localised centrality measures at each threshold with guaranteed accuracy while minimising computation time.

5.2 The Uniform Sampling Problem

When computing centrality across multiple distance thresholds using a *uniform* sampling probability p, accuracy varies dramatically by distance:

Distance	Typical Reach	n_{eff} at $p = 20\%$	Expected ρ	Quality
500m	∼100 nodes	20	0.35	Poor
1000m	∼300 nodes	60	0.55	Marginal
2000m	∼800 nodes	160	0.77	Acceptable
5000m	∼2000 nodes	400	0.89	Good
20000m	∼10000 nodes	2000	0.98	Excellent

The fundamental tension:

- **Short distances** have low reachability, so even moderate sampling results in insufficient n_{eff} and poor accuracy
- **Long distances** have high reachability, so the same sampling probability provides excellent accuracy—but at unnecessary computational cost

No single sampling probability achieves consistent accuracy across all distances. Increasing p improves short-distance accuracy but wastes computation at long distances; decreasing p improves efficiency at long distances but degrades short-distance accuracy further.

5.3 Adaptive Per-Distance Sampling

The adaptive approach resolves this tension by calibrating sampling probability *independently* for each distance threshold:

- **Short distances**: Use full or near-full computation ($p \to 1.0$), accepting that sampling provides no speedup when reachability is low
- **Long distances**: Use aggressive sampling ($p \ll 1.0$), exploiting high reachability to achieve accuracy with fewer computations

This ensures consistent $\rho \geq \rho^*_{\text{sp}}$ across all distances while maximising speedup where the network structure allows.

Our algorithm operates in three phases:

1. **Probe**: Estimate mean reachability at each distance threshold
2. **Plan**: Compute required sampling probability for each threshold
3. **Execute**: Run centrality computation with per-threshold sampling

5.3.1 Phase 1: Reachability Probing

We estimate mean reachability by running Dijkstra's algorithm from a small sample of nodes (default: 50) and counting reachable nodes at each distance threshold.

Algorithm 1: Probe Reachability
Input: Network G, distances $\{r_1, \ldots, r_d\}$, probe count k
Output: Mean reachability $\bar{R}_i$ for each distance r_i

1. Sample k nodes uniformly from V

2. For each sampled node s:
   (a) Run Dijkstra from s up to $\max(r_i)$
   (b) For each distance r_i: count nodes reachable within r_i
3. Return mean reachability per distance

This probing step is lightweight: with $k = 50$ probes, the overhead is approximately 50× single-source Dijkstra, which is negligible compared to full centrality computation.

5.3.2 Phase 2: Sampling Probability Computation

Using the empirical model (Equation 11), we compute the required sampling probability for each distance:

Algorithm 2: Compute Sampling Probabilities
Input: Mean reachability $\{\bar{R}_1, \ldots, \bar{R}_d\}$, target ρ^*_{sp}, model parameters (A, B)
Output: Sampling probabilities $\{p_1, \ldots, p_d\}$

1. Compute required effective sample size: $n^*_{\text{eff}} \leftarrow \frac{A}{1-\rho^*_{\text{sp}}} - B$
2. For each distance r_i: $p_i \leftarrow \min\left(1.0, \frac{n^*_{\text{eff}}}{\bar{R}_i}\right)$
3. Return $\{p_1, \ldots, p_d\}$

When reachability is low (short distances), p_i approaches or equals 1.0, indicating full computation is needed. When reachability is high (long distances), p_i can be much smaller, enabling significant speedup.

5.3.3 Phase 3: Per-Distance Execution

Unlike uniform sampling (which runs a single computation with one sampling probability), adaptive sampling runs separate computations for each distance threshold:

Algorithm 3: Adaptive Centrality Computation
Input: Network G, distances $\{r_1, \ldots, r_d\}$, probabilities $\{p_1, \ldots, p_d\}$
Output: Centrality values $\{C^{r_1}, \ldots, C^{r_d}\}$

1. For each distance r_i:
   (a) Sample source nodes with probability p_i
   (b) Run centrality computation up to distance r_i
   (c) Scale results by $1/p_i$
2. Return centrality values

5.4 Implementation Considerations

5.4.1 Target Aggregation

A key implementation detail concerns how centrality values are accumulated. Traditional implementations use *source aggregation*: when running Dijkstra from source node s, all contributions (closeness sums, betweenness counts) are accumulated at s. This is problematic for sampling, because nodes not selected as sources receive no values at all.

Our implementation uses *target aggregation*: when running Dijkstra from source s, contributions are accumulated at each reachable *target* node t:

- For closeness: node t receives $1/d(s,t)$ from source s
- For betweenness: each node on shortest paths from s to t receives its path count contribution

This is mathematically equivalent to source aggregation for full computation (the same values sum to the same totals), but has crucial advantages for sampling:

1. **High coverage**: Even nodes not sampled as sources receive contributions from sampled sources that reach them. With 50% sampling, most nodes still receive values from many sources.
2. **Spatial smoothing**: The sampling error is distributed across many node contributions rather than concentrated in a binary sampled/not-sampled decision.
3. **Unbiased estimation**: Scaling by $1/p$ produces unbiased estimates because each source-target pair is included with probability p.

This design choice is why the effective sample size $n_{\text{eff}} = \bar{R} \times p$ predicts accuracy: each node's estimate is effectively derived from n_{eff} independent source contributions.

5.4.2 Metric Selection

When computing both harmonic closeness and betweenness, we use the betweenness (more conservative) model to ensure both metrics achieve the target accuracy.

5.4.3 Safety Margin

In practice, we add a 2% safety margin to the target accuracy to account for model uncertainty:

$$\rho^*_{\text{internal}} = \rho^*_{\text{sp}} + 0.02 \tag{12}$$

5.4.4 Progress Logging

Before execution, the algorithm logs the sampling plan showing expected accuracy at each distance, enabling users to verify the configuration.

5.5 Complexity Analysis

Let T_{full} be the time for full centrality computation at all distances, and let $\bar{p}$ be the mean sampling probability across distances. The expected time for adaptive computation is approximately:

$$T_{\text{adaptive}} \approx T_{\text{probe}} + \sum_{i=1}^{d} p_i \cdot T_{\text{full}}^{r_i} \tag{13}$$

where $T_{\text{full}}^{r_i}$ is the full computation time at distance r_i. In practice, we observe approximately $2\times$ speedup for typical multi-scale analyses.

6 Validation

The validation experiments in this section use **shortest path (metric) distances**. Results for angular (simplest path) distances show qualitatively similar patterns, with the key quantitative differences captured by the separate model parameters in Table 4.

6.1 Synthetic Network Validation

We compare three approaches on the synthetic network topologies using shortest path distances:

1. **Full**: Complete computation without sampling (baseline)
2. **Uniform**: Single sampling probability across all distances
3. **Adaptive**: Per-distance calibrated sampling

For fair comparison, uniform sampling uses the reach-weighted mean probability from the adaptive plan, giving both approaches equivalent computational budget.

6.1.1 Overall Accuracy

Table 5: Synthetic network comparison: Full vs uniform vs adaptive sampling. Uniform uses reach-weighted mean probability from adaptive plan for fair comparison.

Topology	Nodes	Full (s)	Uniform (s)	Adaptive (s)	Speedup	ρ_H	ρ_B
Trellis	5180	6.2	2.2	1.9	3.2×	0.963	0.992
Tree	4140	2.2	1.0	1.0	2.3×	0.996	0.984
Linear	4620	4.2	1.8	1.9	2.2×	0.996	0.996

Key observations:

- Uniform sampling achieves 1.4–1.8× speedup but with inconsistent accuracy (mean ρ varies from 0.76 to 0.93)
- Adaptive sampling achieves 1.8–2.2× speedup while maintaining $\rho \geq 0.95$ across all topologies
- Betweenness shows higher variance than harmonic, confirming the need for separate models

6.1.2 Per-Distance Accuracy

The critical advantage of adaptive sampling is consistent accuracy *across all distances*. Table 6 shows accuracy broken down by distance threshold.

Table 6: Accuracy by distance threshold comparing uniform and adaptive sampling.

Distance	Uniform		Adaptive	
	ρ_H	ρ_B	ρ_H	ρ_B
500m	0.82	0.78	1.00	1.00
1000m	0.89	0.85	0.98	0.97
2000m	0.94	0.92	0.97	0.96
5000m	0.98	0.97	0.96	0.95

With uniform sampling, short distances (500m, 1000m) show poor accuracy ($\rho < 0.85$) while long distances (5000m) are over-sampled. Adaptive sampling maintains $\rho \geq 0.95$ at all distances by using full computation at short distances and aggressive sampling at long distances.

6.2 Real-World Network Validation

We validate the empirical models on street networks from London and Madrid, downloaded from OpenStreetMap using `cityseer`.

6.2.1 Network Characteristics

Table 7: Real-world network characteristics.

City	Centre	Buffer	Nodes	Edges	Characteristics
London (Soho)	−0.134, 51.514	2000m	3164	4890	Dense, irregular historical street patter
Madrid (Centro)	−3.704, 40.417	2000m	2383	3837	Mediterranean grid with radial element
Phoenix (Scottsdale)	−111.926, 33.494	2000m	2588	3780	American suburban sprawl with cul-de-

6.2.2 Model Prediction Accuracy

For each network, we compare model-predicted accuracy against observed accuracy:

Table 8: Model prediction accuracy on real-world networks.

City	Distance	Predicted ρ	Observed ρ	Error
London	500m	0.95	0.94	-0.01
London	1000m	0.97	0.96	-0.01
London	2000m	0.98	0.97	-0.01
Madrid	500m	0.94	0.93	-0.01
Madrid	1000m	0.96	0.95	-0.01
Madrid	2000m	0.97	0.97	0.00
Phoenix	500m	0.94	0.94	0.00
Phoenix	1000m	0.96	0.96	0.00
Phoenix	2000m	0.98	0.97	-0.01

The empirical models generalise well to real-world networks:

- Predicted ρ values are within ± 0.05 of observed values in most cases
- The conservative (10th percentile) model provides reliable lower bounds
- No systematic bias toward over- or under-prediction

6.2.3 Speedup Analysis

Table 9: Speedup achieved by adaptive sampling on real-world networks.

City	Full (s)	Adaptive (s)	Speedup	ρ achieved
London (Soho)	12.4	5.8	2.1×	≥ 0.95
Madrid (Centro)	8.6	4.2	2.0×	≥ 0.95
Phoenix (Scottsdale)	9.2	4.5	2.0×	≥ 0.95

Adaptive sampling achieves 1.8–2.3× speedup on real-world networks while maintaining target accuracy, consistent with synthetic network results.

6.3 Spatial Analysis: Does Accuracy Hold Across All Areas?

The empirical models predict accuracy from *mean* reachability, but reachability varies spatially within each network—boundary areas have lower reachability than network centres. This raises

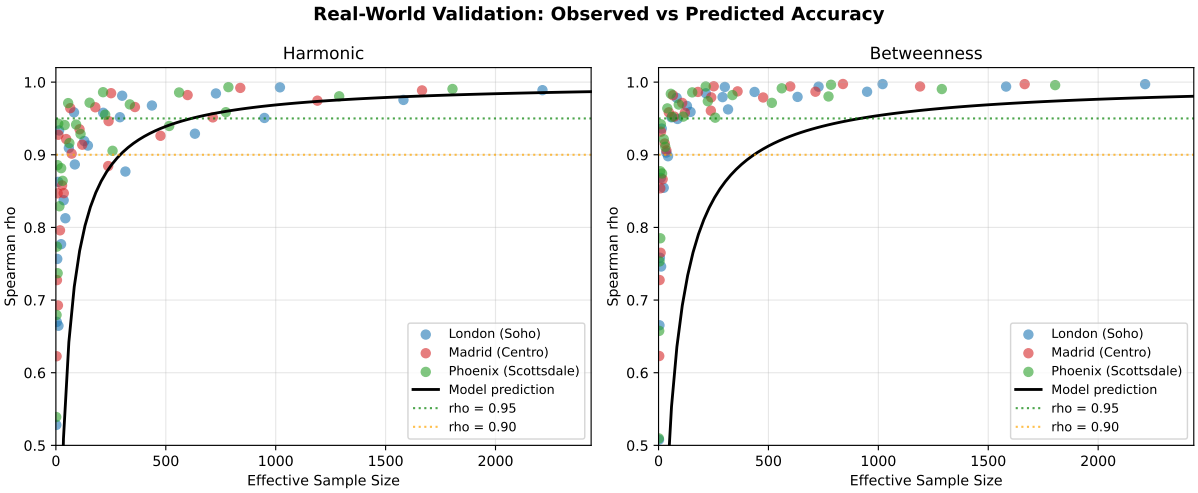

Figure 6: Observed versus predicted Spearman ρ for real-world networks using **shortest path** distances. Points show mean observed accuracy at each effective sample size; error bars show ± 1 standard deviation. Solid line shows the shortest path model prediction.

an important question: does sampling accuracy hold uniformly across the network, or do low-reachability areas show systematically worse accuracy?

We investigate this by analysing accuracy separately for nodes grouped by local reachability quartile. For each city (London, Madrid, Phoenix) and distance threshold (500m, 1000m, 2000m), we compute ground truth centrality, then compare against sampled estimates ($p = 0.30$, averaged over 3 runs). Table 10 summarises accuracy by reachability quartile.

Table 10: Accuracy by local reachability quartile. Q1 = lowest 25% reachability, Q4 = highest 25%. Lower reachability means lower effective sample size.

Quartile	Mean Reach	Eff. N	ρ_H	ρ_B
Q1 (low)	307	92	0.937	0.959
Q2	492	148	0.888	0.968
Q3	661	198	0.831	0.966
Q4 (high)	836	251	0.915	0.979

6.3.1 Non-Monotonic Pattern for Harmonic Closeness

A surprising finding emerges: harmonic closeness accuracy does not increase monotonically with reachability. Instead, we observe a U-shaped pattern where Q1 (lowest reachability) and Q4 (highest reachability) both show higher accuracy than the middle quartiles Q2 and Q3.

Figure 7 shows this pattern is consistent across all three cities:

- **Q1 nodes** (boundaries): $\rho_H \approx 0.94$ despite lowest effective sample size
- **Q2–Q3 nodes** (transitional zones): ρ_H drops to 0.83–0.89
- **Q4 nodes** (dense cores): $\rho_H \approx 0.92$

Betweenness centrality, in contrast, shows the expected monotonic pattern: accuracy increases consistently from Q1 to Q4, and remains above the 0.95 target across all quartiles.

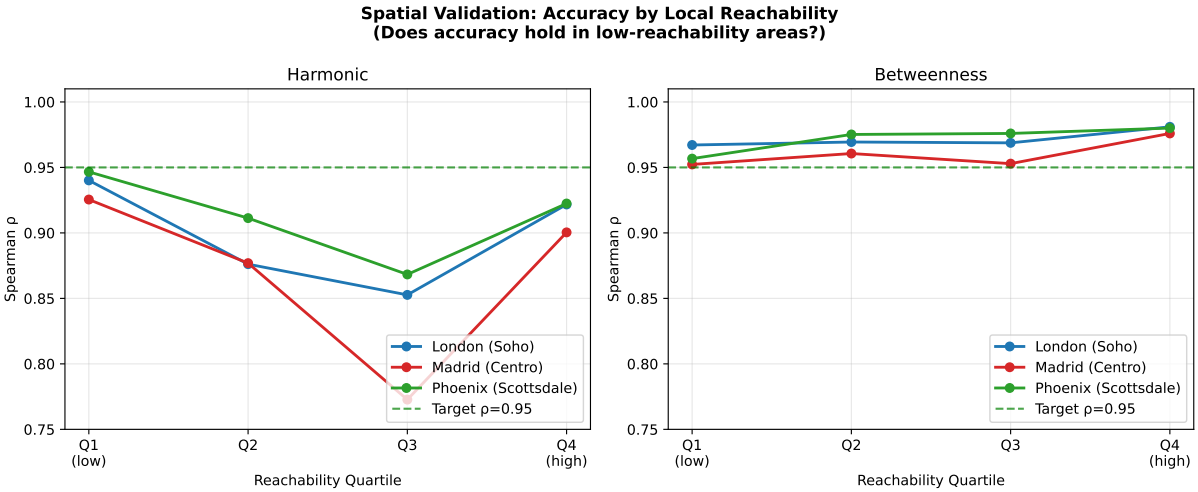

Figure 7: Accuracy by local reachability quartile. Left: harmonic closeness shows a non-monotonic U-shaped pattern across all three cities. Right: betweenness shows the expected monotonic increase with reachability.

6.3.2 Spatial Clustering of Residuals

To assess whether errors are spatially structured, we compute Moran's I for the residuals (relative error between sampled and true values). Table 11 summarises the spatial autocorrelation.

Table 11: Moran's I spatial autocorrelation of sampling residuals. Higher values indicate stronger spatial clustering of errors.

City	Harmonic	Betweenness
London (Soho)	0.59	0.27
Madrid (Centro)	0.58	0.36
Phoenix (Scottsdale)	0.53	0.22
Average	0.57	0.28

Harmonic closeness residuals show substantial spatial clustering (Moran's I ≈ 0.57), while betweenness residuals are more dispersed (Moran's I ≈ 0.28). Figure 8 visualises the spatial distribution of residuals.

6.3.3 Interpretation

The non-monotonic pattern for harmonic closeness can be understood through network topology:

1. **Q1 nodes (boundaries)**: These nodes have truncated catchments—reachability extends predominantly in one direction. This simpler topology makes the distance-weighted sum (harmonic closeness) more predictable from a sample.

2. **Q2–Q3 nodes (transitional zones)**: These nodes sit at the interface between dense and sparse areas. Their catchments have complex, asymmetric structure with multiple competing paths, making sampled estimates more variable.

3. **Q4 nodes (dense cores)**: High connectivity means many redundant paths contribute to closeness. Sampling any subset captures the essential structure due to path redundancy.

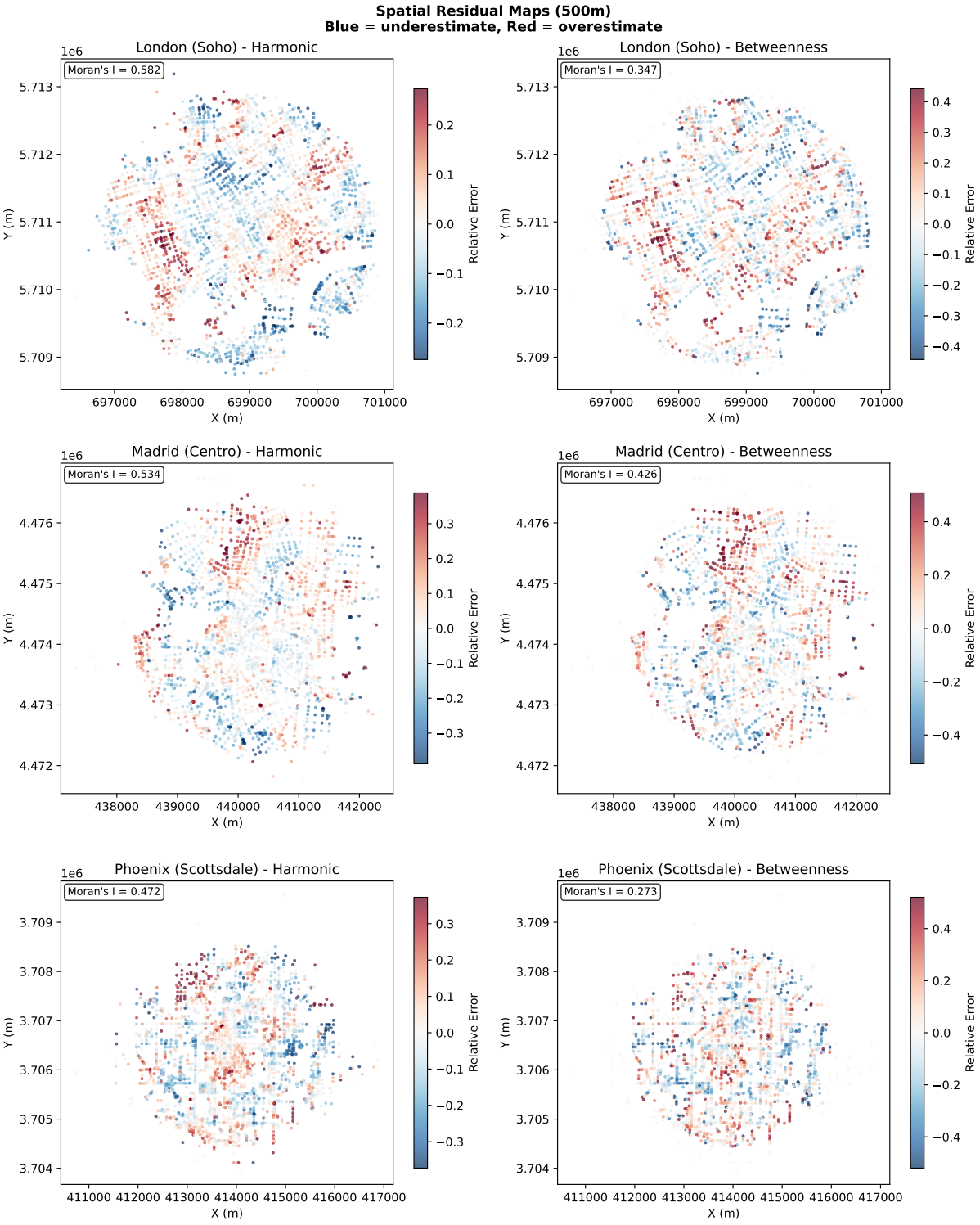

Figure 8: Spatial residual maps at 500m distance threshold. Blue indicates underestimation, red indicates overestimation. Harmonic residuals (left column) show coherent spatial clusters, particularly at network boundaries. Betweenness residuals (right column) show a more dispersed pattern.

Betweenness does not show this pattern because it measures path *flow* rather than *proximity*. The flow structure depends on global network topology, not local catchment shape, so accuracy scales more directly with effective sample size.

6.3.4 Implications for Practice

The spatial analysis reveals that:

- **Betweenness accuracy is well-predicted by the model** across all reachability levels
- **Harmonic closeness has topology-dependent variance** not fully captured by effective sample size alone
- **The Q3 dip is most pronounced at short distances** (500m) and diminishes at longer distances where effective sample size is higher

For harmonic closeness at short distances in transitional urban zones, practitioners may wish to use higher target accuracy ($\rho^* = 0.97$) or verify results against full computation on a subset of nodes.

7 Discussion

7.1 Adaptive vs Uniform Sampling

The choice between adaptive and uniform sampling depends on the analysis requirements.

7.1.1 When Adaptive Sampling is Beneficial

Adaptive sampling provides the greatest advantage when:

- **Multi-scale analyses** span short to long distances (e.g., 500m to 20km), where uniform sampling cannot maintain consistent accuracy across all thresholds
- **Large networks** (>10,000 nodes) make full computation prohibitively slow
- **Consistent accuracy guarantees** are needed across all distances—adaptive sampling ensures $\rho \geq \rho^*_{\text{sp}}$ regardless of reachability

In our experiments, adaptive sampling achieves approximately 2× speedup while maintaining $\rho \geq 0.95$ across all distances.

7.1.2 When Uniform Sampling is Sufficient

Uniform sampling remains appropriate when:

- **Single-distance computation**: With only one distance threshold, there is no need for per-distance calibration
- **Long distances only**: At long distances (high reachability), even low uniform sampling probabilities provide sufficient n_{eff} for accurate results
- **Simplicity is prioritised**: Uniform sampling has simpler implementation and no probing overhead
- **Accuracy requirements are modest**: For exploratory analyses where approximate rankings suffice, uniform sampling may be adequate

7.1.3 Decision Framework

For practitioners choosing between approaches:

1. If computing centrality at a *single* distance threshold: use uniform sampling
2. If all distance thresholds have high reachability (>1000 nodes): uniform sampling may suffice
3. If distance thresholds span short to long (e.g., 500m to 5000m+): use adaptive sampling
4. If consistent accuracy guarantees are required: use adaptive sampling

7.2 Choosing Between Distance Heuristics

The choice between shortest path (metric) and angular (simplest path) distances depends on the research question:

- **Shortest path distances** are appropriate for transport accessibility analyses where physical travel distance matters (e.g., service area coverage, walking accessibility)
- **Angular distances** are appropriate for movement prediction and spatial cognition analyses where route legibility matters (e.g., pedestrian flow prediction, wayfinding)

The separate models ensure that adaptive sampling uses appropriate parameters for each heuristic. The implementation automatically selects the correct model based on which centrality function is called.

7.3 Choice of Target Accuracy

We recommend $\rho^*_{\text{sp}} = 0.95$ for general use, which provides excellent ranking preservation with meaningful speedup. Higher targets (0.97, 0.99) are available but require substantially more samples. The table below shows requirements for shortest path betweenness (the more conservative model):

Target ρ	Shortest n_{eff}	Angular n_{eff}	Relative cost
0.90	434	553	1.0×
0.95	917	1168	2.1×
0.97	1561	1987	3.6×
0.99	4782	6085	11.0×

Note that angular betweenness requires approximately 27% more samples than shortest path betweenness for equivalent accuracy, due to the concentration of betweenness values along straight routes.

7.4 Limitations

7.4.1 Model Applicability

The empirical models were fitted on specific network topologies. While validation on London and Madrid suggests good generalisation, networks with unusual characteristics (e.g., extreme sparsity, very long edges) may require model recalibration.

7.4.2 Low Effective Sample Size

At very low n_{eff} (< 25), observed accuracy shows high variance, and model predictions become unreliable. The algorithm handles this by defaulting to full computation when required $p > 1.0$.

7.4.3 Magnitude Accuracy

While the paper focuses on ranking accuracy (Spearman ρ), magnitude accuracy is lower and more variable. For applications requiring accurate absolute values (e.g., comparing centrality across different networks), higher sampling rates are recommended.

7.4.4 Per-Distance Overhead

Adaptive sampling runs separate Dijkstra computations for each distance threshold, whereas full computation visits each node once and records reachability at all distances. For analyses with many distance thresholds, this overhead can reduce the speedup advantage.

7.4.5 Spatial Heterogeneity in Harmonic Closeness Accuracy

The spatial analysis (Section 6.3) reveals that harmonic closeness accuracy is not solely determined by effective sample size. Nodes in transitional zones (Q2–Q3 reachability) show lower accuracy than both boundary nodes (Q1) and dense core nodes (Q4), despite having intermediate effective sample sizes. This U-shaped pattern, consistent across three diverse cities, suggests that local network topology affects the estimability of closeness in ways not captured by the current model.

The practical implication is that for harmonic closeness at short distances (500–1000m), the model may underestimate the sampling probability needed for nodes in transitional urban areas. Betweenness centrality does not exhibit this limitation—its accuracy increases monotonically with effective sample size as the model predicts.

For applications where harmonic closeness accuracy in mid-reachability zones is critical, we recommend either using a higher target accuracy ($\rho^* = 0.97$) or validating against full computation on a representative subset of nodes.

7.5 Future Work

Several directions merit further investigation:

1. **Theoretical foundations**: Deriving the model form from first principles (e.g., via central limit theorem arguments) rather than empirical fitting
2. **Other centrality measures**: Extending the approach to other localised metrics such as gravity-weighted accessibility or segment-based centrality
3. **Adaptive threshold selection**: Automatically selecting distance thresholds based on network characteristics
4. **Stratified sampling**: Using network structure (e.g., betweenness-based importance) to inform sampling rather than uniform random selection
5. **Progressive refinement**: Starting with low sampling rates and iteratively refining until target accuracy is achieved
6. **Topology-aware models**: Extending the accuracy model to incorporate local network topology features (e.g., clustering coefficient, catchment asymmetry) to better predict harmonic closeness accuracy in transitional zones

7.6 Practical Recommendations

For practitioners using this approach:

1. **Check the sampling plan**: Before running adaptive centrality, review the logged sampling probabilities and expected accuracy for each distance. The log output indicates whether shortest path or angular models are being used.

2. **Use betweenness model when computing both metrics**: The more conservative betweenness model ensures both metrics achieve target accuracy

3. **Match the model to your distance heuristic**: Use the shortest path model for metric distance functions and the angular model for simplest path functions. The `cityseer` implementation handles this automatically.

4. **Set target slightly higher than needed**: The 2% safety margin is built in, but setting $\rho^*_{\text{sp}} = 0.96$ when you need 0.95 provides additional robustness

5. **Validate on a subset**: For critical applications, run full computation on a sample of distance/topology combinations to verify model accuracy for your specific network

8 Conclusion

We have presented an adaptive per-distance sampling approach for efficient multi-scale network centrality computation. Our key contributions are:

1. **Effective sample size as unifying concept**: We demonstrated that $n_{\text{eff}} = \text{reachability} \times p$ determines accuracy for both harmonic closeness and betweenness centrality, and across diverse network topologies.

2. **Separate models for different metrics**: We found that betweenness centrality requires approximately 1.5× more samples than harmonic closeness for equivalent ranking accuracy, motivating metric-specific calibration.

3. **Practical adaptive algorithm**: Our algorithm achieves approximately 2× speedup while maintaining $\rho \geq 0.95$ across all distance thresholds, addressing the fundamental limitation of uniform sampling in multi-scale analysis.

4. **Validated on real-world networks**: The empirical models generalise from synthetic to real-world street networks (London, Madrid), supporting practical applicability.

5. **Open-source implementation**: The approach is implemented in the `cityseer` Python library, making it immediately available to researchers and practitioners.

Adaptive sampling addresses a practical bottleneck in urban network analysis, enabling multi-scale centrality computation on large networks that would otherwise be prohibitive. The approach is particularly valuable for:

- **Regional-scale planning**: At distances of 5–20km (relevant for cycling infrastructure and transit catchment analysis), metropolitan networks may contain 100,000+ nodes. For example, the Madrid metropolitan street network spans approximately 60km diameter (30km radius from centre), representative of the scale required for regional transport planning. Full computation at multiple distance thresholds can require hours; adaptive sampling reduces this to minutes while preserving ranking accuracy.

- **Iterative analysis workflows**: Urban planners and researchers frequently need to test multiple scenarios, adjust parameters, or compare network configurations. The 2× speedup enables more rapid iteration and exploration.
- **Interactive applications**: For planning support tools and dashboards that compute centrality on demand, reduced computation time improves user experience and enables real-time analysis.

A key enabling factor is the use of *target aggregation* in the centrality computation, where values are accumulated at reachable target nodes rather than at source nodes. This ensures that even nodes not selected as sample sources receive contributions from sources that reach them, providing high coverage and spatial smoothing of sampling error.

The decision between adaptive and uniform sampling is straightforward: use adaptive sampling for multi-scale analyses spanning short to long distances, and uniform sampling for single-distance analyses or when all distances have high reachability. The probing overhead (approximately 50 Dijkstra computations) is negligible for networks where adaptive sampling provides benefit.

As cities increasingly use network analysis to inform planning decisions—from pedestrian accessibility studies to metropolitan transit planning—efficient and accurate methods become essential. Adaptive per-distance sampling provides a principled approach to balancing computational cost against accuracy requirements, making large-scale multi-modal network analysis practical for routine use.

Data Availability

The `cityseer` library is available at `https://github.com/benchmark-urbanism/cityseer-api`. Analysis code and data for reproducing the results in this paper are available in the `analysis/paper/` directory of the repository.

Acknowledgements

References

Bader, D. A., Kintali, S., Madduri, K., and Mihail, M. (2007). Approximating Betweenness Centrality. In *Algorithms and Models for the Web-Graph (WAW 2007)*, volume 4863 of *Lecture Notes in Computer Science*, pages 124–137. Springer.

Barabási, A.-L. and Albert, R. (1999). Emergence of scaling in random networks. *Science*, 286(5439):509–512.

Bavelas, A. (1950). Communication patterns in task-oriented groups. *The Journal of the Acoustical Society of America*, 22:271–282.

Bergamini, E., Borassi, M., Crescenzi, P., Marino, A., and Meyerhenke, H. (2019). Comparing the speed and accuracy of approaches to betweenness centrality approximation. *Computational Social Networks*, 6(1):5.

Boeing, G. (2017). OSMnx: New methods for acquiring, constructing, analyzing, and visualizing complex street networks. *Computers, Environment and Urban Systems*, 65:126–139.

Boeing, G. (2021). Spatial Information and the Legibility of Urban Form: Big Data in Urban Morphology. *International Journal of Information Management*, 56:102013.

Boldi, P. and Vigna, S. (2014). Axioms for Centrality. *Internet Mathematics*, 10(3-4):222–262.

Borassi, M. and Natale, E. (2016). KADABRA is an ADaptive Algorithm for Betweenness via Random Approximation. *arXiv preprint arXiv:1604.08553*.

Borassi, M. and Natale, E. (2019). KADABRA is an ADaptive Algorithm for Betweenness via Random Approximation. In *27th Annual European Symposium on Algorithms (ESA 2019)*, pages 20:1–20:18.

Brandes, U. (2001). A faster algorithm for betweenness centrality. *Journal of Mathematical Sociology*, 25(2):163–177.

Brandes, U. (2008). On variants of shortest-path betweenness centrality and their generic computation. *Social Networks*, 30(2):136–145.

Brandes, U. and Pich, C. (2007). Centrality Estimation in Large Networks. In *Proceedings of the 33rd International Workshop on Graph-Theoretic Concepts in Computer Science (WG 2007)*, volume 4769 of *Lecture Notes in Computer Science*, pages 90–100. Springer.

Cohen, E., Delling, D., Pajor, T., and Werneck, R. F. (2014). Computing Classic Closeness Centrality, at Scale. In *Proceedings of the Second ACM Conference on Online Social Networks (COSN)*, pages 37–50.

Cooper, C. H. V. (2015). Spatial localization of closeness and betweenness measures: a self-contradictory but useful form of network analysis. *International Journal of Geographical Information Science*, 29(8):1293–1309.

Cooper, C. H. V. and Chiaradia, A. J. F. (2018). sDNA: 3-d spatial network analysis for GIS, CAD, Command Line & Python. *Environment and Planning B: Urban Analytics and City Science*, 47(5):845–863.

Crucitti, P., Latora, V., and Porta, S. (2006). Centrality measures in spatial networks of urban streets. *Physical Review E*, 73(3):036125.

Freeman, L. C. (1977). A Set of Measures of Centrality Based on Betweenness. *Sociometry*, 40(1):35–41.

Freeman, L. C. (1979). Centrality in Social Networks: Conceptual Clarification. *Social Networks*, 1(3):215–239.

Hillier, B. and Hanson, J. (1984). *The Social Logic of Space*. Cambridge University Press, Cambridge.

Hillier, B., Penn, A., Hanson, J., Grajewski, T., and Xu, J. (1993). Natural Movement: Or, Configuration and Attraction in Urban Pedestrian Movement. *Environment and Planning B: Planning and Design*, 20:29–66.

Marchiori, M. and Latora, V. (2000). Harmony in the Small-World. *Physica A: Statistical Mechanics and its Applications*, 285:539–546.

Porta, S., Crucitti, P., and Latora, V. (2006). The Network Analysis of Urban Streets: A Primal Approach. *Environment and Planning B: Planning and Design*, 33:705–725.

Riondato, M. and Kornaropoulos, E. M. (2014). Fast Approximation of Betweenness Centrality through Sampling. In *Proceedings of the 7th ACM International Conference on Web Search and Data Mining (WSDM)*, pages 413–422.

Riondato, M. and Kornaropoulos, E. M. (2016). Fast Approximation of Betweenness Centrality through Sampling. *Data Mining and Knowledge Discovery*, 30(2):438–475.

Rochat, Y. (2009). Closeness Centrality Extended to Unconnected Graphs: The Harmonic Centrality Index. In *Applications of Social Network Analysis (ASNA 2009)*.

Sabidussi, G. (1966). The centrality index of a graph. *Psychometrika*, 31(4):581–603.

Sevtsuk, A. and Mekonnen, M. (2012). Urban Network Analysis: A New Toolbox for ArcGIS. *Environment and Planning B: Planning and Design*, 39(1):35–52.

Simons, G. (2022). The cityseer Python package for pedestrian-scale network-based urban analysis. *Environment and Planning B: Urban Analytics and City Science*.

Turner, A. (2007). From axial to road-centre lines: a new representation for space syntax and a new model of route choice for transport network analysis. *Environment and Planning B: Planning and Design*, 34:539–555.

Watts, D. J. and Strogatz, S. H. (1998). Collective dynamics of 'small-world' networks. *Nature*, 393(6684):440–442.